



Light (anti-)nuclei and (anti-)hypertriton production in pp collisions at $\sqrt{s} = 0.90, 2.76$ and 7 TeV

Nserdin A. Ragab^{1,2}, Zhi-Lei She^{1,2}, Gang Chen^{1,a}

¹ School of Mathematics and Physics, China University of Geosciences, Wuhan 430074, China

² Institute of Geophysics and Geomatics, China University of Geosciences, Wuhan 430074, China

Received: 26 May 2020 / Accepted: 29 August 2020 / Published online: 17 September 2020

© Società Italiana di Fisica and Springer-Verlag GmbH Germany, part of Springer Nature 2020

Abstract Production of light (anti-)nuclei and (anti-)hypertriton within midrapidity ($|y| < 0.5$) and $p_T < 3.0$ GeV/c in pp interactions at $\sqrt{s} = 0.90, 2.76$ and 7 TeV is investigated by the dynamically constrained phase space coalescence model, combined with PACIAE model. The ALICE data for yields, ratios, as well as transverse momentum distributions of \bar{d} and d are well reproduced by the model simulations, meanwhile the three basic characters of ${}^3\bar{\text{He}}$, ${}^3\text{He}$, ${}^3_{\Lambda}\bar{\text{H}}$, and ${}^3_{\Lambda}\text{H}$ are also predicted. Besides, we found the yields of light (anti-)nuclei produced are dependent upon their mass number A , namely, their yields sharply decrease with the increasing of A . The strangeness population factor $s_3 = ({}^3_{\Lambda}\text{H}/{}^3\text{He})/(\Lambda/p)$ is found to be about 0.7–0.8, and is comparable with the available experimental results.

1 Introduction

The investigation of anti-nuclei is a hot and frontier topic in particle and nuclear physics, cosmology, and astrophysics. Since plentiful nuclei and anti-nuclei can be produced in high energy accelerator experiment, it exactly provides a chance to study light (anti-)nuclei production [1].

In the last decades, production of antimatter has been a focus in several collision systems under different energies. In large systems, the light anti-nuclei (e.g., \bar{d} , ${}^3\bar{\text{He}}$, even ${}^4\bar{\text{He}}$) and anti-hypertriton (${}^3_{\Lambda}\bar{\text{H}}$) have been successfully measured, such as in Au–Au collisions [2–5] within $\sqrt{s_{NN}} = 7.7$ GeV to 200 GeV and in Pb–Pb interactions [6–9] at $\sqrt{s_{NN}} = 2.76$ TeV, respectively. For the little systems, ALICE Collaboration has also published papers on light anti-nuclei production in pp interactions [6, 7, 10] at $\sqrt{s} = 0.90, 2.76$, and 7 TeV.

Theoretically, one can normally select several numerical models (e.g., a transport model) to predict the production of (anti-)nucleons and (anti-)hyperons. Then, light (anti-)nuclei and (anti-)hypernuclei production are computed with a statistical method [11] or a certain phase-space coalescence model [12–15]. As examples some researches applied the selected coalescence model to combine a multiphase transport (AMPT) model [16] or the blast-wave approach [17–19], to study light (anti-)nuclei production in high energy nuclear-nuclear collisions. Besides those efforts, the DCPC model [20, 21] was created to investigate production of light (anti-)nuclei [22, 23] in high energy pp collisions [24] and nucleus-nucleus (Pb–

^a e-mail: chengangl@cug.edu.cn (corresponding author)

Pb [25], and Au-Au [26], Cu-Cu [27]) collisions, in which the final state hadrons produced within parton and hadron cascade model (PACIAE) [28].

In this work, we generate final-state hadrons produced by the PACIAE model in high energy pp collisions (non-single diffractive (NSD) process) at three separate center-of-mass (c.m.) energies. Next, the DCPC model was applied to study production of light nuclei (d , ${}^3\text{He}$ and ${}^3_{\Lambda}\text{H}$) and their corresponding anti-nuclei (\bar{d} , ${}^3\bar{\text{He}}$, and ${}^3_{\Lambda}\bar{\text{H}}$). In Sect. 2, we have introduced the PACIAE model and DCPC model briefly. In Sect. 3, the model simulations are shown. The Sect. 4 presents a concise plot summary.

2 Models

Based on the PYTHIA6.4 model [29], the PACIAE [28] is promoted to mainly study the hadron-hadron and nucleus-nucleus collisions, relying on the collision geometry and nucleon-nucleon (NN) total cross section. In the PACIAE model the strings at this stage will randomly break into free partons, forming the partonic initial state. Then parton rescattering is introduced using the $2 \rightarrow 2$ (LO-pQCD) interaction cross sections of parton-parton [30]. After parton rescattering the hadronization then proceeds [28, 29, 31]. At last, a hadron rescattering is introduced, in which the two-body collision method [32, 33] is applied, until all hadrons have reached freeze-out.

We generated the final-state particles by PACIAE model [28], and then hadrons are processed with DCPC model [20] to build light (anti)nuclei. Considering the uncertainty principle in quantum statistical mechanics [34],

$$\Delta \mathbf{q} \Delta \mathbf{p} \geq h^3, \quad (1)$$

one can only know that a particle (positions \mathbf{q} and momentum \mathbf{p}) lies somewhere within a volume of $\Delta \mathbf{q} \Delta \mathbf{p}$ or state inside a quantum “box” occupied a volume (h^3) of six-dimension phase space [21]. Then one could define an integral to directly evaluate the yield for a single particle:

$$Y_1 = \int_{H \leq E} \frac{d\mathbf{q}d\mathbf{p}}{h^3}. \quad (2)$$

Here, H is the Hamiltonian, E denotes the energy of the particle. Likewise, the yield for N particles could be valued with

$$Y_N = \int \dots \int_{H \leq E} \frac{d\mathbf{q}_1 d\mathbf{p}_1 \dots d\mathbf{q}_N d\mathbf{p}_N}{(h^3)^N}. \quad (3)$$

While Eq. (3) should satisfy the following constraint conditions:

$$\begin{aligned} |\mathbf{q}_{ij}| &\leq D_0, \quad (i \neq j; i, j = 1, 2, 3, \dots, N), \\ m_0 - \Delta m &\leq m_{inv} \leq m_0 + \Delta m, \end{aligned} \quad (4)$$

where

$$m_{inv} = \sqrt{(E_1 + E_2 + E_3)^2 - (\mathbf{p}_1 + \mathbf{p}_2 + \mathbf{p}_3)^2}, \quad (5)$$

$|\mathbf{q}_{ij}|$ denotes the distance between particles j th and i th, D_0 and m_0 are the diameter and rest mass of N particles cluster, respectively. p_i and E_i ($i = 1, 2, 3$) represent the momenta and energies of particles, respectively. Δm stands for the allowed uncertainty. In Eq. (3), the integral of continuous distributions will be changed by using the sum for discrete distributions,

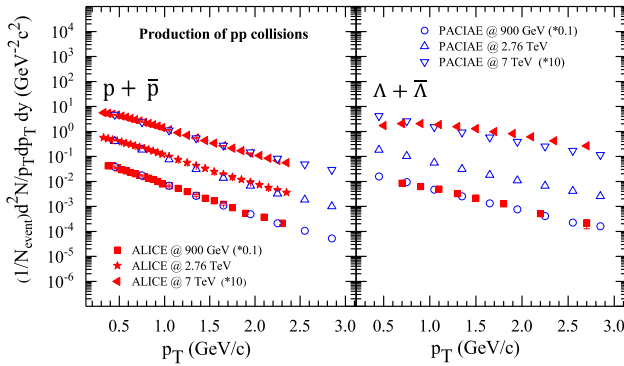


Fig. 1 The transverse momentum (p_T) distribution of $p + \bar{p}$ and $\Lambda + \bar{\Lambda}$ in mid-rapidity pp collisions at c.m. energy of 0.90, 2.76 and 7 TeV, calculated by PACIAE model. The data have been multiplied by constant factors inside the figure. The ALICE data are taken from [35–37,40]

because the hadron momentum and position distributions are discrete in transport model simulation.

3 Results and discussion

We generate the final-state hadrons by the transport model PACIAE. Then utilize the DCPC model to coalescence production of light (anti-)nuclei [20]. The model parameters are fixed on the default values given in PYTHIA6.4. However, the K factor as well as the parameters $parj(1)$, $parj(2)$, and $parj(3)$ were roughly fitted the (anti-)proton and $\Lambda(\bar{\Lambda})$ from ALICE data in mid-rapidity pp collisions at $\sqrt{s} = 0.90, 2.76$ and 7 TeV [35–37,40], as shown in Fig. 1. It shows that the results of PACIAE simulation are very close to the ALICE data. The parameters were chosen from Fig. 1 as $parj(1) = 0.07$ (default value is 0.10), $parj(2) = 0.18$ (0.30), $parj(3) = 0.40$ (0.40), with $K = 0.95$ (1.0 or 1.5), which were applied to compute the yields of $d, \bar{d}, {}^3\text{He}, {}^3\bar{\text{He}}, {}^3_\Lambda\text{H},$ and ${}^3_\Lambda\bar{\text{H}}$, in mid-rapidity pp collisions of the c.m. energy of 0.90, 2.76 and 7 TeV relying on the final-state hadrons from the PACIAE simulations. The consequence of light (anti-)nuclei yields are shown in Table 1.

Table 1 shows that:

- The yield computed by PACIAE model of ${}^3_\Lambda\text{H}({}^3_\Lambda\bar{\text{H}})$ is significantly less than that of ${}^3\text{He}({}^3\bar{\text{He}})$, since the yield of hyperons is less than that of protons.
- When the c.m. energy varies from 900 GeV to 7 TeV, the (anti-)proton yield calculated by PACIAE simulations increases $\sim 50\%$. That is less than the increase of light (anti-)nuclei (over 100% for d and \bar{d} , $\sim 60\%$ for ${}^3\text{He}$ and ${}^3\bar{\text{He}}$). Here, the yields of $d(pn)$ and ${}^3\text{He}(ppn)$ produced by nucleon combination will inevitably increase when the c. m. energy of pp collision increases and the number of final nucleons increases. However, this may attribute to a larger increase of available phase space for anti-nuclei production than that for anti-hadron production.
- The yield of d and \bar{d} calculated by PACIAE+DCPC simulation nicely matches the ALICE data in the range of uncertainty. Meanwhile, we predict the yield of ${}^3\text{He}, {}^3\bar{\text{He}}, {}^3_\Lambda\text{H},$ and ${}^3_\Lambda\bar{\text{H}}$ in rapidity pp collisions at c.m. energy of 0.90, 2.76 and 7 TeV using PACIAE+DCPC model.

Table 1 The yields of (anti-)particles in mid-rapidity pp collisions at c.m. energy of 0.90, 2.76 and 7 TeV calculated by PACIAE + DCPC simulations, compared with the ALICE data [10, 35–38, 40]

| Particle | PACIAE + DCPC | | | ALICE | | |
|--------------------------------|------------------|------------------|------------------|-----------------------------|-----------------------------|-----------------------------|
| | 0.90 TeV | 2.76 TeV | 7 TeV | 0.90 TeV | 2.76 TeV | 7 TeV |
| p | 0.082 | 0.090 | 0.124 | 0.083 ± 0.008 | 0.090 ± 0.007 | 0.124 ± 0.009 |
| \bar{p} | 0.079 | 0.088 | 0.122 | 0.079 ± 0.008 | 0.088 ± 0.006 | 0.123 ± 0.010 |
| Λ | 0.048 | 0.060 | 0.087 | 0.048 ± 0.005 | – | 0.090 ± 0.007 |
| $\bar{\Lambda}$ | 0.047 | 0.060 | 0.086 | 0.047 ± 0.007 | – | 0.089 ± 0.006 |
| d | $1.06\text{E-}4$ | $1.41\text{E-}4$ | $2.04\text{E-}4$ | $(1.12 \pm 0.13)\text{E-}4$ | $(1.53 \pm 0.14)\text{E-}4$ | $(2.02 \pm 0.17)\text{E-}4$ |
| \bar{d} | $9.83\text{E-}5$ | $1.35\text{E-}4$ | $1.98\text{E-}4$ | $(1.11 \pm 0.13)\text{E-}4$ | $(1.37 \pm 0.13)\text{E-}4$ | $(1.92 \pm 0.15)\text{E-}4$ |
| ${}^3\text{He}$ | $5.17\text{E-}8$ | $7.79\text{E-}8$ | $1.16\text{E-}7$ | – | – | – |
| ${}^3\bar{\text{He}}$ | $4.62\text{E-}8$ | $7.28\text{E-}8$ | $1.10\text{E-}7$ | – | – | $(1.10 \pm 0.63)\text{E-}7$ |
| ${}^3_{\Lambda}\text{H}$ | $2.36\text{E-}8$ | $3.69\text{E-}8$ | $5.62\text{E-}8$ | – | – | – |
| ${}^3_{\Lambda}\bar{\text{H}}$ | $2.06\text{E-}8$ | $3.32\text{E-}8$ | $5.23\text{E-}8$ | – | – | – |

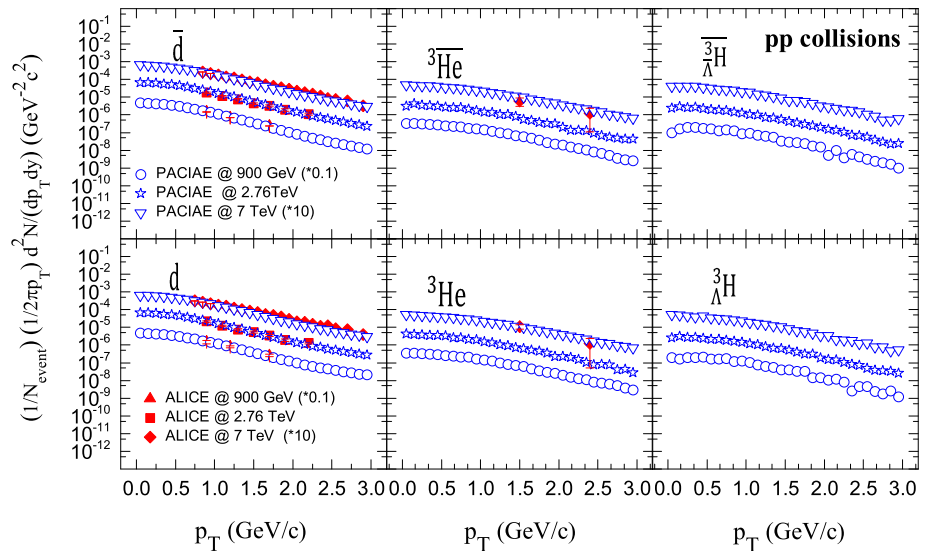


Fig. 2 The transverse momentum distribution of d , \bar{d} , ${}^3\text{He}$, ${}^3\bar{\text{He}}$, ${}^3_{\Lambda}\text{H}$, and ${}^3_{\Lambda}\bar{\text{H}}$ computed by PACIAE+DCPC simulations in rapidity pp collisions at c.m. energy of 0.90, 2.76 and 7 TeV. The solid points are ALICE data [10]; for clarity, the data are separated with multiplying constant factors here

It should be noted that the yield of d and \bar{d} is simulated with the parameter $\Delta m = 0.003$ GeV, and the yield of ${}^3_{\Lambda}\text{H}$ (${}^3_{\Lambda}\bar{\text{H}}$) and ${}^3\text{He}$ (${}^3\bar{\text{He}}$) is simulated with the parameter $\Delta m = 0.0075$ GeV. The parameter Δm for d (\bar{d}) and ${}^3\text{He}$ (${}^3\bar{\text{He}}$, ${}^3_{\Lambda}\text{H}$, ${}^3_{\Lambda}\bar{\text{H}}$) are determined by fitting the yield of d and ${}^3\text{He}$ with ALICE experimental data in pp collisions at c.m. energy of 7 TeV [10], respectively.

Figure 2 presents the spectrum of integral yields for d (\bar{d}), ${}^3\text{He}$ (${}^3\bar{\text{He}}$), and ${}^3_{\Lambda}\text{H}$ (${}^3_{\Lambda}\bar{\text{H}}$) calculated by PACIAE+DCPC model with $p_T < 3$ GeV/c, $|y| < 0.5$ in pp collisions at

Table 2 The top part show the ratio of anti-particles (\bar{p} , $\bar{\Lambda}$, \bar{d} , ${}^3\bar{\text{He}}$, and ${}^3_{\Lambda}\bar{\text{H}}$) to particles (p , Λ , d , ${}^3\text{He}$, and ${}^3_{\Lambda}\text{H}$) in rapidity pp collisions at $\sqrt{s} = 0.90, 2.76$ and 7 TeV, then display the mixed ratios between different (anti-)particles

| Particle | PACIAE + DCPC | | | ALICE | | |
|---|------------------|------------------|------------------|------------------------------|------------------------------|------------------------------|
| | 0.90 TeV | 2.76 TeV | 7 TeV | 0.90 TeV | 2.76 TeV | 7 TeV |
| \bar{p}/p | 0.963 | 0.978 | 0.984 | 0.952 ± 0.002 | 0.978 ± 0.002 | 0.992 ± 0.009 |
| $\bar{\Lambda}/\Lambda$ | 0.981 | 0.993 | 0.984 | 0.963 ± 0.023 | 0.979 ± 0.015 | 0.989 ± 0.014 |
| \bar{d}/d | 0.927 | 0.954 | 0.967 | 0.991 ± 0.09 | 0.895 ± 0.05 | 0.950 ± 0.02 |
| ${}^3\bar{\text{He}}/{}^3\text{He}$ | 0.893 | 0.935 | 0.948 | – | – | – |
| ${}^3_{\Lambda}\bar{\text{H}}/{}^3_{\Lambda}\text{H}$ | 0.873 | 0.909 | 0.925 | – | – | – |
| d/p | $1.29\text{E}-3$ | $1.57\text{E}-3$ | $1.65\text{E}-3$ | $(1.38 \pm 0.186)\text{E}-3$ | $(1.48 \pm 0.167)\text{E}-3$ | $(1.63 \pm 0.170)\text{E}-3$ |
| \bar{d}/\bar{p} | $1.24\text{E}-3$ | $1.53\text{E}-3$ | $1.62\text{E}-3$ | $(1.39 \pm 0.205)\text{E}-3$ | $(1.31 \pm 0.145)\text{E}-3$ | $(1.56 \pm 0.170)\text{E}-3$ |
| ${}^3\text{He}/d$ | $4.88\text{E}-4$ | $5.52\text{E}-4$ | $5.69\text{E}-4$ | – | – | – |
| ${}^3\bar{\text{He}}/\bar{d}$ | $4.70\text{E}-4$ | $5.39\text{E}-4$ | $5.56\text{E}-4$ | – | – | $(5.73 \pm 3.26)\text{E}-4$ |
| Λ/p | 0.585 | 0.667 | 0.702 | 0.578 ± 0.082 | – | 0.726 ± 0.077 |
| $\bar{\Lambda}/\bar{p}$ | 0.595 | 0.670 | 0.705 | 0.595 ± 0.107 | – | 0.724 ± 0.076 |
| ${}^3_{\Lambda}\text{H}/{}^3\text{He}$ | 0.456 | 0.474 | 0.484 | – | – | – |
| ${}^3_{\Lambda}\bar{\text{H}}/{}^3\bar{\text{He}}$ | 0.446 | 0.456 | 0.475 | – | – | – |

On the bottom the ratios of $\Lambda(\bar{\Lambda})$ to $p(\bar{p})$ and ${}^3_{\Lambda}\text{H}({}^3_{\Lambda}\bar{\text{H}})$ to ${}^3\text{He}({}^3\bar{\text{He}})$ are presented. ALICE data are from Ref. [10,35–38,40]

$\sqrt{s} = 0.90, 2.76$ and 7 TeV, individually. One can see the transverse momentum spectrum of $d, \bar{d}, {}^3\text{He}, {}^3\bar{\text{He}}$ calculated by PACIAE+DCPC simulations is consistent with the result distribution of ALICE data [10]. Then we predict the whole distribution of the transverse momentum spectrum of ${}^3\text{He}, {}^3\bar{\text{He}}, {}^3_{\Lambda}\text{H}$, and ${}^3_{\Lambda}\bar{\text{H}}$ in pp collisions at these three separate energies, respectively (Table 2).

Considering high energy collisions, the nature of light (anti-)nuclei production mechanism is final-state hadron coalescence, therefore the yield ratios of nuclei can be predicted through the coalescence model. In theory, the yield ratios for two (anti-)nuclei could be straightly compared with yield ratios of constituent hadrons in the naive coalescence framework [17,39]. For example, the ratio of ${}^3_{\Lambda}\bar{\text{H}}/{}^3_{\Lambda}\text{H}$ is supposed to proportional to $(\bar{\Lambda}/\Lambda)(\bar{p}/p)(\bar{n}/n)$, due to ${}^3_{\Lambda}\bar{\text{H}}$ and ${}^3_{\Lambda}\text{H}$ are individually generated by $(\bar{p} + \bar{n} + \bar{\Lambda})$ and $(p + n + \Lambda)$. Hence one can write the yield ratios as follows:

$$\frac{{}^3_{\Lambda}\bar{\text{H}}}{{}^3_{\Lambda}\text{H}} = \frac{\bar{p}\bar{n}\bar{\Lambda}}{pn\Lambda} \simeq \left(\frac{\bar{p}}{p}\right)^2 \frac{\bar{\Lambda}}{\Lambda}, \tag{6}$$

once again, mixed ratios like that:

$$\frac{{}^3_{\Lambda}\text{H}}{{}^3\text{He}} = \frac{pn\Lambda}{ppn} \simeq \frac{\Lambda}{p}. \tag{7}$$

The yield ratio of anti-particles (\bar{p} , $\bar{\Lambda}$, \bar{d} , ${}^3\bar{\text{He}}$ and ${}^3_{\Lambda}\bar{\text{H}}$) to their corresponding particles (p , Λ , d , ${}^3\text{He}$, and ${}^3_{\Lambda}\text{H}$) and their mixed ratios ($\Lambda/p, \bar{\Lambda}/\bar{p}, {}^3_{\Lambda}\text{H}/{}^3\text{He}, {}^3_{\Lambda}\bar{\text{H}}/{}^3\bar{\text{He}}$) in pp collisions at $\sqrt{s} = 0.90, 2.76$ and 7 TeV are presented in Table II. Obviously, we can obtain the ratios

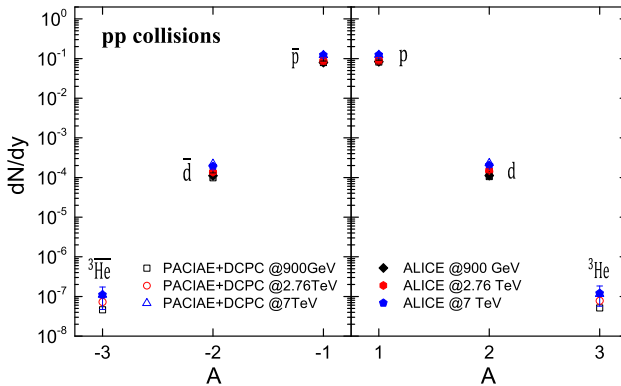


Fig. 3 Integrated yields of anti-nuclei (left section) and nuclei (right section) in mid-rapidity pp collisions at $\sqrt{s} = 0.90, 2.76$ and 7 TeV, vary with atomic mass number A . And PACIAE+DCPC model (see open point) results are displayed. The ALICE data (solid point) is taken from [10,35–38]

of anti-nuclei and anti-hypertriton to nuclei and hypertriton are all dependent on the c.m. energy, as same as their yields increase with the c.m. energy increase as Table I shown. One also find the ratios of anti-particles to their corresponding particles, and (anti-)hypertriton to (anti-)helium-3 (${}^3_{\Lambda}\text{H}/{}^3\text{He}$, $\frac{{}^3_{\Lambda}\bar{\text{H}}/{}^3\bar{\text{He}}}{\bar{\Lambda}}$) are less than 1, and the latter implies yield of ${}^3_{\Lambda}\text{H}(\frac{{}^3_{\Lambda}\bar{\text{H}}}{\bar{\Lambda}})$ is less than that of ${}^3\text{He}(\frac{{}^3\bar{\text{H}}}{\bar{\Lambda}})$.

As the above Eq. (6) shows, since the constituent hadrons of $\frac{{}^3_{\Lambda}\bar{\text{H}}}{\bar{\Lambda}}$ and $\frac{{}^3_{\Lambda}\text{H}}{\Lambda}$ are $(\bar{\Lambda} + \bar{p} + \bar{n})$ and $(\Lambda + p + n)$ in coalescence model, the yield ratio of $\frac{{}^3_{\Lambda}\bar{\text{H}}/{}^3_{\Lambda}\text{H}}$ is proportional to $(\frac{\bar{p}}{p})^2 \frac{\bar{\Lambda}}{\Lambda}$. And then the ratios \bar{d} to d are consistent with $(\bar{p}/p)^2$, the ratios $\frac{{}^3_{\Lambda}\bar{\text{H}}/{}^3\bar{\text{He}}}{\bar{\Lambda}}$ is approximately the same as $(\bar{p}/p)^3$, and the ratios $\frac{{}^3_{\Lambda}\bar{\text{H}}/{}^3_{\Lambda}\text{H}}$ is just approximately $(\bar{p}^2 \bar{\Lambda})/(p^2 \Lambda)$ as Table II shows. The calculated $\frac{{}^3_{\Lambda}\bar{\text{H}}/{}^3_{\Lambda}\text{H}}$ values well matched the theoretical assumption that $\frac{{}^3_{\Lambda}\bar{\text{H}}}{\bar{\Lambda}}$ and $\frac{{}^3_{\Lambda}\text{H}}{\Lambda}$ are individually generated with hadrons coalescence of $(\bar{\Lambda} + \bar{p} + \bar{n})$ and $(\Lambda + p + n)$. Furthermore, the simulation consequences (\bar{d}/d) in our model are found to be comparable with the experimental data from ALICE Collaboration in mid-rapidity pp collisions at $\sqrt{s} = 0.90, 2.76$ and 7 TeV, respectively.

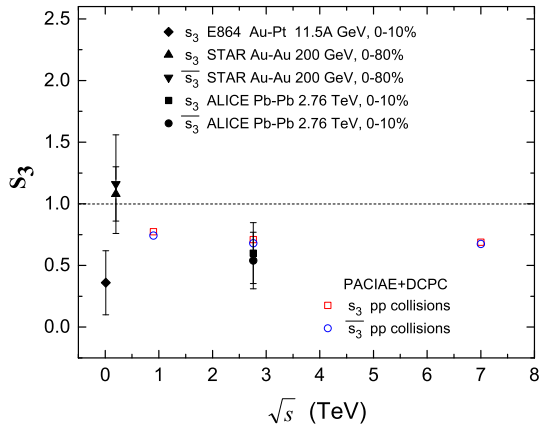
To further understand the mass and/or c.m. energy dependence of production of light (anti-)nuclei, Fig. 3 gives integrated yield distributions of light anti-nuclei ($\bar{p}, \bar{d}, {}^3\bar{\text{He}}$) and nuclei ($p, d, {}^3\text{He}$), versus the atomic mass number $A(A = 1$ to $3)$ in different c.m. energy of $0.90, 2.76$ and 7 TeV, respectively. The hollow points denote our results computed using PACIAE+DCPC simulation in mid-rapidity pp collisions at LHC energies, with $p_T < 3.0$ GeV/c and $|y| < 0.5$. The solid points show the data of ALICE experiment [10,35–38]. We can find from Fig. 3 yields of light (anti-)nuclei decrease sharply as atomic mass number A increase. Numerically, integrated yield of light (anti-)nuclei spans about 3-orders of magnitude with noteworthy exponential type. Besides, Fig. 3 shows that PACIAE+DCPC simulations are consistent with the data from ALICE within uncertainties.

In order to better compare (anti-)hypernuclei with (anti-)nuclei, by analogy with heavy-ion collisions, the strangeness population factor [9,41] in pp collisions can also be introduced as follows:

$$s_3 = ({}^3_{\Lambda}\text{H} \times p)/({}^3\text{He} \times \Lambda) \tag{8}$$

$$\bar{s}_3 = (\frac{{}^3_{\Lambda}\bar{\text{H}}}{\bar{\Lambda}} \times \bar{p})/(\frac{{}^3\bar{\text{H}}}{\bar{\Lambda}} \times \bar{\Lambda}). \tag{9}$$

Fig. 4 The $s_3(\bar{s}_3)$ value as a function of \sqrt{s} in pp interactions computed by PACIAE+DCPC model. Here the data from STAR [5], ALICE [9], and E864 [41] are also presented, and error bars denote statistical uncertainties



Note that, the proton and antiproton here does not include the contribution of $\Lambda(\bar{\Lambda})$ decay to proton and antiproton. The s_3 value is likely to study production mechanism for light nuclei in high energy collisions [14, 42], due that it's quite related to local baryon-strangeness correlation [43–45]. The $s_3(\bar{s}_3)$ values in pp collisions computed by PACIAE+DCPC model for three separate c.m. energies of 0.90, 2.76 and 7 TeV are presented in Fig. 4. The present results for pp collisions show the values of $s_3(\bar{s}_3)$ are about 0.7–0.8. Furthermore, the calculated $s_3(\bar{s}_3)$ values are compared with the results from STAR [5], ALICE [9], and E864 [41], and are consistent with experiment data within uncertainties allowed.

It should be noted that the statistical error of the predicted results calculated by the model is not written, since it is very small and can be ignored.

4 Conclusion

The production of light (anti-)nuclei and (anti-)hypertriton has been studied by the DCPC model, relied on the final-state hadrons created by the PACIAE model within $|y| < 0.5$ and $p_T < 3$ GeV/c in mid-rapidity pp collisions at c.m. energy of 0.90, 2.76 and 7 TeV, respectively. The basic variable simulation includes yield, yield ratio, transverse momentum spectrum of $d, \bar{d}, {}^3\text{He}, \bar{{}^3\text{He}}, {}^3_\Lambda\text{H}$ and $\bar{{}^3}_\Lambda\text{H}$.

The results of our calculations show a significant dependence of the c.m. energy on yield, ratio, and transverse momentum distribution for $d, \bar{d}, {}^3\text{He}, \bar{{}^3\text{He}}, {}^3_\Lambda\text{H}$ and $\bar{{}^3}_\Lambda\text{H}$. When the c.m. energy varies from 900 GeV to 7 TeV, yield of light (anti-)nuclei and (anti-)hypertriton computed with PACIAE+DCPC simulation increases. The ratios of \bar{d} to $d, \bar{{}^3\text{He}}$ to ${}^3\text{He}$, and $\bar{{}^3}_\Lambda\text{H}$ to ${}^3_\Lambda\text{H}$ all approach unity with c.m. energies increase, indicating nuclei and anti-nuclei species are produced with similar abundance at LHC energies. The ALICE data for yield, ratio, as well as spectrum of \bar{d} and d are well reproduced with PACIAE+DCPC simulations. We also obtained yields of light (anti-)nuclei decrease sharply when atomic mass number A increases. The strangeness population factor $s_3 = ({}^3_\Lambda\text{H}/{}^3\text{He})/(\Lambda/p)$ for (anti-)hypertriton with (anti-)helium-3 is calculated to be about 0.7–0.8, which is compatible with the experimental data.

The data used to support the findings of this study are included within the article. The authors declare that they have no conflicts of interest.

Acknowledgements The work is supported by the NSFC of China under Grant No. 11475149. This work is also supported by the high-performance computing platform of China University of Geosciences.

References

1. J.H. Chen, D. Keane, Y.G. Ma et al., Antinuclei in heavy-ion collisions. *Phys. Rep.* **760**, 1 (2018)
2. S.S. Adler et al., (PHENIX Collaboration), Deuteron and antideuteron production in Au+Au Collisions at $\sqrt{s_{NN}} = 200$ GeV. *Phys. Rev. Lett.* **94**, 122302 (2005)
3. W.J. Llope for the STAR Collaboration, Light (anti-)nucleus production in $\sqrt{s_{NN}} = 7.7\text{--}200$ GeV Au-Au collisions in the STAR Experiment, 2012. <http://meetings.aps.org/link/BAPS.2012.DNP.HB.4>
4. H. Agakishiev et al., (STAR Collaboration), Observation of the antimatter helium-4 nucleus. *Nature* **473**, 353 (2011)
5. B.I. Abelev et al., (STAR Collaboration), Observation of an antimatter hypernucleus. *Science* **328**, 58 (2010)
6. N. Sharma et al., (ALICE Collaboration), Production of nuclei and antinuclei in pp and Pb–Pb collisions with ALICE at the LHC. *J. Phys. G: Nucl. Part. Phys.* **38**, 124189 (2011)
7. J. Adam et al., (ALICE Collaboration), Production of light nuclei and anti-nuclei in pp and Pb–Pb collisions at energies available at the CERN Large Hadron Collider. *Phys. Rev. C* **93**, 024917 (2016)
8. S. Acharya et al. (ALICE Collaboration), Production of ${}^4\text{He}$ and ${}^4\bar{\text{He}}$ in Pb–Pb collisions at $\sqrt{s_{NN}} = 2.76$ TeV at the LHC, *Nucl. Phys. A* **971**, 1–20, 2018
9. J. Adam et al. (ALICE Collaboration), ${}^3_\Lambda\text{H}$ and ${}^3_{\bar{\Lambda}}\text{H}$ production in Pb–Pb collisions at $\sqrt{s_{NN}} = 2.76$ TeV, *Phys. Lett. B* **754**, 360, 2016
10. S. Acharya et al. (ALICE Collaboration), Production of deuterons, tritons, ${}^3\text{He}$ nuclei, and their antinuclei in pp collisions at $\sqrt{s} = 0.9, 2.76$, and 7 TeV, *Phys. Rev. C* **97**, 024615, 2018
11. V. Topor Pop, S. Das Gupta, Model for hypernucleus production in heavy ion collisions, *Phys. Rev. C* **81**, 054911, (2010)
12. R. Mattiello, H. Sorge, H. Stöcker et al., Nuclear clusters as a probe for expansion flow in heavy ion reactions at (10–15)A GeV. *Phys. Rev. C* **55**, 1443 (1997)
13. L.W. Chen, C.M. Ko, Φ And Ω production in relativistic heavy-ion collisions in a dynamical quark coalescence model. *Phys. Rev. C* **73**, 044903 (2006)
14. S. Zhang, J.H. Chen, H. Crawford et al., Searching for onset of deconfinement via hypernuclei and baryon-strangeness correlations. *Phys. Lett. B* **684**, 224 (2010)
15. P. Liu, J.H. Chen, Y.G. Ma et al., Production of light nuclei and hypernuclei at High Intensity Accelerator Facility energy region. *Nucl. Sci. Tech.* **28**, 55 (2017)
16. L.L. Zhu, C.M. Ko, X.J. Yin, Light (anti-)nuclei production and flow in relativistic heavy-ion collisions. *Phys. Rev. C* **92**, 064911 (2015)
17. L. Xue, Y.G. Ma, J.H. Chen et al., Production of light (anti-)nuclei, (anti-)hypertriton, and di- Λ in central Au + Au collisions at energies available at the BNL Relativistic Heavy Ion Collider. *Phys. Rev. C* **85**, 064912, (2012)
18. C.S. Zhou, Y.G. Ma, S. Zhang, Scaling of nuclear modification factors for hadrons and light nuclei. *Eur. Phys. J. A* **52**, 354 (2016)
19. N. Shah, Y.G. Ma, J.H. Chen et al., Production of multistrange hadrons, light nuclei and hypertriton in central Au+Au collisions at $\sqrt{s_{NN}} = 11.5$ and 200 GeV, *Phys. Lett. B* **754**, 6, (2016)
20. Y.L. Yan, G. Chen, X.M. Li et al., Predictions for the production of light nuclei in pp collisions at $\sqrt{s} = 7$ and 14 TeV. *Phys. Rev. C* **85**, 024907 (2012)
21. G. Chen, Y.L. Yan, D.S. Li et al., Antimatter production in central Au + Au collisions at $\sqrt{s_{NN}} = 200$ GeV. *Phys. Rev. C* **86**, 054910 (2012)
22. G. Chen, H. Chen, J. Wu et al., Centrality dependence of light (anti-)nuclei and (anti-)hypertriton production in Au + Au collisions at $\sqrt{s_{NN}} = 200$ GeV. *Phys. Rev. C* **88**, 034908 (2013)
23. G. Chen, H. Chen, J.L. Wang et al., Scaling properties of light (anti-)nuclei and (anti-)hypertriton production in Au+Au collisions at $\sqrt{s_{NN}} = 200$ GeV. *J. Phys. G: Nucl. Part. Phys.* **41**, 115102 (2014)
24. J.L. Wang, D.K. Li, H.J. Li et al., The energy dependence of antiparticle to particle ratios in high energy pp collisions. *Int. J. Mod. Phys. E* **23**, 1450088 (2014)
25. Z.L. She, G. Chen, H.G. Xu et al., Centrality dependence of light (anti-)nuclei and (anti-)hypertriton production in Pb–Pb collisions at $\sqrt{s_{NN}} = 2.76$ TeV, *Eur. Phys. J. A* **52**, 93, (2016)
26. Z.J. Dong, Q.Y. Wang, G. Chen et al., Energy dependence of light (anti-)nuclei and (anti-)hypertriton production in the Au-Au collision from $\sqrt{s_{NN}} = 11.5$ to 5020 GeV, *Eur. Phys. J. A* **54**, 144, (2018)

27. F.X. Liu, G. Chen, Z.L. She et al., ${}^3_{\Lambda}H$ and ${}^3_{\Lambda}\overline{H}$ production and characterization in Cu + Cu collisions at $\sqrt{s_{NN}} = 200$ GeV. Phys. Rev. C **99**, 034904 (2019)
28. B.H. Sa, D.M. Zhou, Y.L. Yan et al., PACIAE 2.0: An updated parton and hadron cascade model (program) for the relativistic nuclear collisions, Comput. Phys. Commun. **183**, 333, (2012)
29. T. Sjöstrand, S. Mrenna, P. Skands, PYTHIA 6.4 physics and manual, J. High Energy Phys. **05**, 026, (2006)
30. B.L. Cambridge, J. Kripfganz, J. Ranft et al., Hadron production at large transverse momentum and QCD. Phys. Lett. B **70**, 234 (1977)
31. Y.L. Yan, D.M. Zhou, B.G. Dong et al., Centrality dependence of forward-backward multiplicity correlation in Au + Au collisions at $\sqrt{s_{NN}} = 200$ GeV. Phys. Rev. C **81**, 044914 (2010)
32. B.H. Sa, A. Tai, An event generator for the firecracker model and the rescattering in high energy pA and AA collisions LUCIAE version 2.0, Comput. Phys. Commun. **90**, 121, (1995)
33. A. Tai, B.H. Sa, LUCIAE 3.0: A new version of a computer program for the Firecracker Model and rescattering in relativistic heavy-ion collisions, Comput. Phys. Commun. **116**, 353, (1999)
34. K. Stowe, *An introduction to thermodynamics and statistical mechanics, Cambridge, 2007* (Statistical Mechanics, North-Holland Publishing Company, Amsterdam, R. Kubo, 1965)
35. B.I. Abelev et al. (ALICE Collaboration), Production of charged pions, kaons and protons at large transverse momenta in pp and Pb–Pb collisions at $\sqrt{s_{NN}} = 2.76$ TeV, Phys. Lett. B **736**, 196–207, (2014)
36. K. Aamodt et al., (ALICE Collaboration), Production of pions, kaons and protons in pp collisions at $\sqrt{s} = 900$ GeV with ALICE at the LHC. Eur. Phys. J. C **71**, 1655 (2011)
37. J. Adam et al., (ALICE Collaboration), Measurement of pion, kaon and proton production in proton-proton collisions at $\sqrt{s} = 7$ TeV. Eur. Phys. J. C **75**, 226 (2015)
38. E. Abbas et al. (ALICE Collaboration), Mid-rapidity anti-baryon to baryon ratios in pp collisions at $\sqrt{s} = 0.9, 2.76$ and 7 TeV measured by ALICE, Eur. Phys. J. C **73**, 2496, (2013)
39. J. Cleymans, S. Kabana, I. Kraus et al., Antimatter production in proton-proton and heavy-ion collisions at ultrarelativistic energies. Phys. Rev. C **84**, 054916 (2011)
40. S. Acharya et al., (ALICE Collaboration), Multiplicity dependence of light-flavor hadron production in pp collisions at $\sqrt{s} = 7$ TeV. Phys. Rev. C **99**, 024906 (2019)
41. T. Armstrong et al. (E864 Collaboration), Production ${}^3_{\Lambda}H$ and ${}^4_{\Lambda}H$ in central 11.5-GeV/c Au+Pt heavy ion collisions, Phys. Rev. C **70**, 024902, (2004)
42. H. Sato, K. Yazaki, On the coalescence model for high energy nuclear reactions. Phys. Lett. B **98**, 153 (1981)
43. V. Koch, A. Majumder, J. Randrup, Baryon-strangeness correlations: a diagnostic of strongly interacting matter. Phys. Rev. Lett. **95**, 182301 (2005)
44. M. Cheng, P. Hegde, C. Jung et al., Baryon number, strangeness and electric charge fluctuations in QCD at high temperature. Phys. Rev. D **79**, 074505 (2009)
45. P. Braun-Munzinger, J. Stachel, The quest for the quark-gluon plasma. Nature **448**, 302 (2007)